Supplementary information for

Twist-angle dependent pseudo-magnetic fields in monolayer $CrCl_2$/graphene heterostructures

Zhengbo Cheng[1#], Nanshu Liu[2#], Jinghao Deng[1], Hui Zhang[1], Zemin Pan[1], Chao Zhu[1], Shuangzan Lu[1,3], Yusong Bai[1], Xiaoyu Lin[1], Wei Ji[2*], Chendong Zhang[1*]

[1]*School of Physics and Technology, Wuhan University, Wuhan 430072, China*

[2]*Beijing Key Laboratory of Optoelectronic Functional Materials and Micro-Nano Devices, Department of Physics, Renmin University of China, Beijing 100872, China*

[3]*Hubei Jiufengshan Laboratory, Wuhan, 430074, China*

[#]*These authors contribute equally to this work.*

**Correspondence and requests for materials should be addressed to:*

wji@ruc.edu.cn (W. J.), cdzhang@whu.edu.cn (C.D. Z)

Supporting note 1. The Landau level spacing is affected by the twist angle.

In graphene superlattices, the structure deformation results in a pseudo-vector potential **A**, which is associated with shear deformation and can be expressed as follows:

$$A_x = c\frac{\beta\gamma_0}{d}(u_{xx} - u_{yy}),$$

$$A_y = -c\frac{2\beta\gamma_0}{d}u_{xy},$$

where d = 1.42 Å represents the equilibrium carbon-carbon distance, $c \approx 1$ is a numerical factor dependent on the specific chemical bond model, $\beta \approx 2$ denotes the electronic Grüneisen parameter, γ_0 = 3.2 eV indicates the strength of first-neighbor interaction in the plane, and u_{ij} signifies the deformation tensor. The PMF is defined as $\mathbf{B} = \nabla \times \mathbf{A}$, which can be approximated to be :

$$|\mathbf{B}| \approx \frac{\hbar c}{e}\left(\frac{2\beta}{3}\right)\frac{\bar{u}}{a_m d},$$

where a_m denotes the diameter of the strain region. The magnitude of the shear deformation, $\bar{u}$, can be computed based on the first neighbor inter-atomic distances in the deformed sample:

$$\bar{u} = \frac{\sqrt{3\left(d_3 - d_2\right)^2 + \left(d_2 + d_3 - 2d_1\right)^2}}{2d},$$

Here, d_1, d_2, and d_3 represent the first neighbor inter-atomic distances in the deformed lattice. Consequently, it can be concluded that PMFs fundamentally arise from lattice deformation.

According to the reference [*ACS Nano* **16**, 1471–1476 (2022)], in the moiré superlattice, the interlayer coupling varies with the twist angle, which subsequently affects the shear deformation resulting from the interlayer coupling. Additionally, as stated in Equation 1, the spacing of the Landau levels is related to the PMF. Consequently, as the rotation angle decreases and interlayer coupling increases, the shear deformation becomes more pronounced, leading to stronger induced PMFs and an increased distance between the Landau levels.

Supplementary Figures

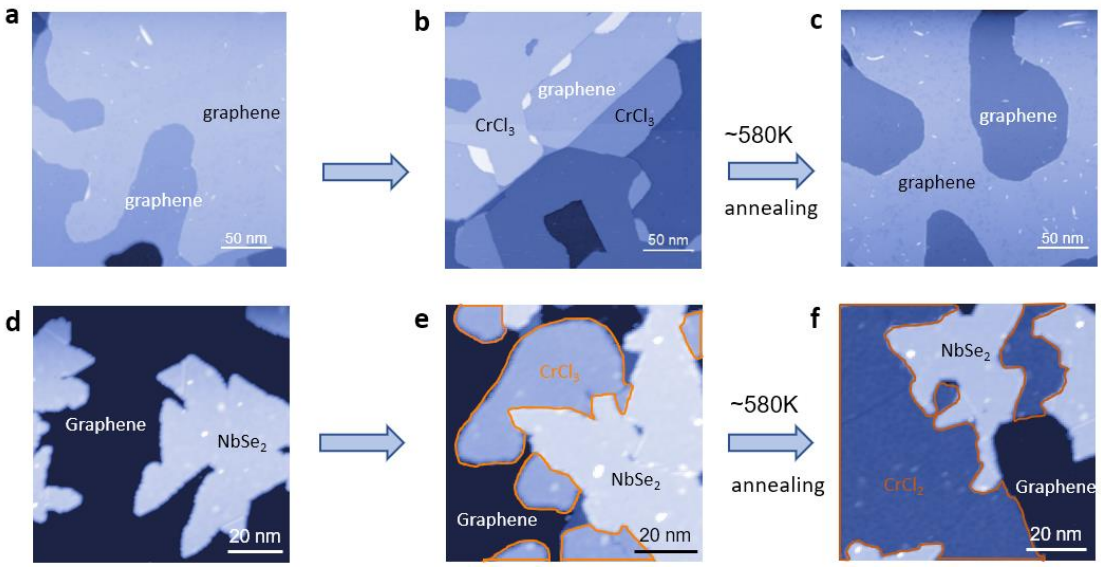

Figure S1 | Fabrication of monolayer $CrCl_2$ on graphene. **a-c**, Directly growth of $CrCl_2$ on graphene. **a**, STM morphology of graphene before growth. **b**, STM morphology after the growth of $CrCl_3$. **c**, STM morphology after annealing. $CrCl_3$ on graphene was completely desorbed, while the formation of $CrCl_2$ was not detected. **d-f**, $NbSe_2$ was grown before $CrCl_2$ growth. **d**, STM morphology of $NbSe_2$ grown on graphene. **e**, STM morphology after the growth of $CrCl_3$. **f**, STM morphology after annealing. $CrCl_3$ on graphene is decomposed into $CrCl_2$. Scanning parameters for all images: V_{bias} = 1.5 V, I_t = 5 pA.

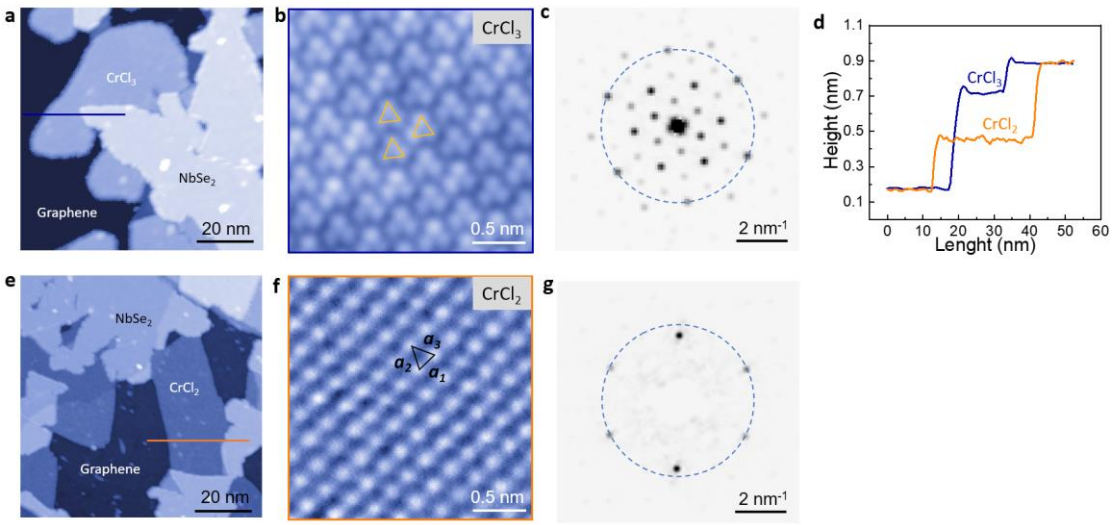

Figure S2 | Morphology and atomic structures of $CrCl_3$ and $CrCl_2$ films. a, Morphology of $CrCl_3$-$NbSe_2$ before annealing (V_{bias} = 1.5 V, I_t = 5 pA). **b**, Atomically resolved images of the monolayer $CrCl_3$ (V_{Bias} = 0.4 V, I_t = 10 pA). **c**, FFT of an atomic resolution image of the monolayer $CrCl_3$. **d**, Line profile of $CrCl_3$-$NbSe_2$ and $CrCl_2$-$NbSe_2$ in (a) and (e). **e**, Morphology of $CrCl_3$-$NbSe_2$ before annealing (V_{bias} = 1.5 V, I_t = 5 pA). **f**, Atomically resolved images of the monolayer $CrCl_3$ (V_{Bias} = 0.4 V, I_t = 10 pA). **g**, FFT of an atomic resolution image of the monolayer $CrCl_2$ lattice. The observed apparent height, morphology, and structural symmetry of the annealed film suggest that $CrCl_3$ decomposes into $CrCl_2$ during the annealing process.

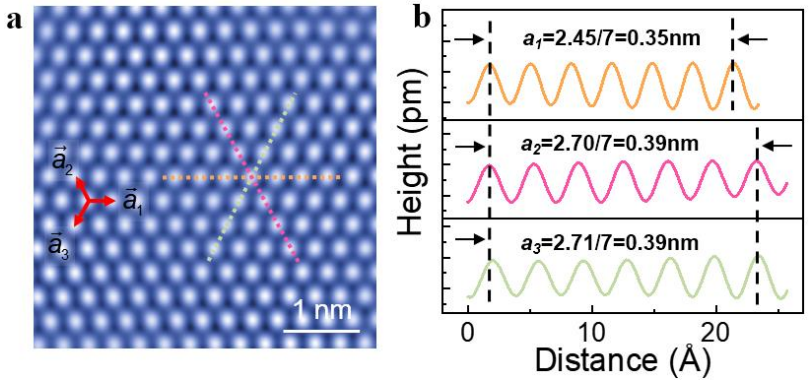

Figure S3 | Determining the lattice constant of $CrCl_2$ in real space. a, Atomically resolved STM images of $CrCl_2$ lattices (FFT-filtered from Fig. 1b). **b**, Line profile of $CrCl_2$ in (a) along $\boldsymbol{a_1}$, $\boldsymbol{a_2}$ and $\boldsymbol{a_3}$.

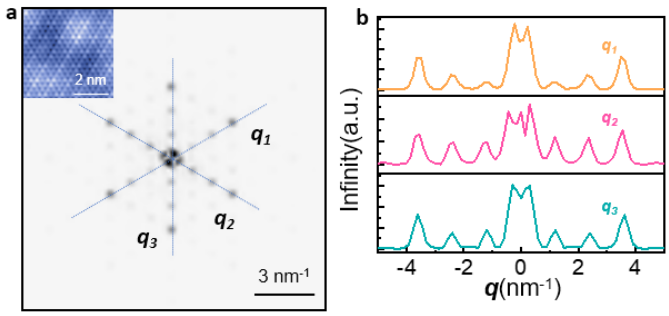

c

	Length(nm^{-1})	Lattice constant a(nm)	Parameter α
q_1	3.7914	0.3447	1
q_2	3.7968	0.3443	α_2=0.99861
q_3	3.8074	0.3431	α_3=0.99527

Figure S4 | Calibration of lattice distortion caused by nonlinearity of the STM scanner. a, FFT of an atomic resolution image of the monolayer $NbSe_2$ lattice (insert), setpoint: V_{Bias} = 0.1V, I_t = 50 pA. **b**, Line profiles along $\boldsymbol{q_1}$, $\boldsymbol{q_2}$ and $\boldsymbol{q_3}$ directions marked in (a). **c**, Calibration of lattice constant with parameter α.

For a two-dimensional crystal lattice with the reciprocal lattice vectors ($\boldsymbol{q_1}$, $\boldsymbol{q_2}$, $\boldsymbol{q_3}$) of the Bravais lattice, its primitive lattice vectors are:

$$\boldsymbol{a_1} = 2\pi \frac{\boldsymbol{q_3} \times \boldsymbol{n}}{\boldsymbol{q_1} \cdot (\boldsymbol{q_3} \times \boldsymbol{n})}$$

$$\boldsymbol{a_2} = 2\pi \frac{\boldsymbol{q_1} \times \boldsymbol{n}}{\boldsymbol{q_2} \cdot (\boldsymbol{q_1} \times \boldsymbol{n})}$$

$$\boldsymbol{a_3} = 2\pi \frac{\boldsymbol{q_2} \times \boldsymbol{n}}{\boldsymbol{q_3} \cdot (\boldsymbol{q_2} \times \boldsymbol{n})}$$

The vector $\boldsymbol{n}$ represents the normal vector of the two-dimensional plane. Combining the measurement results of the reciprocal vector in Fig. S3a with the equations provided above, the lattice constants are determined to be $\boldsymbol{a_1}$ = 0.3447, $\boldsymbol{a_2}$ = 0.3443, and $\boldsymbol{a_3}$ = 0.3431 nm. Consequently, the parameter α is obtained.

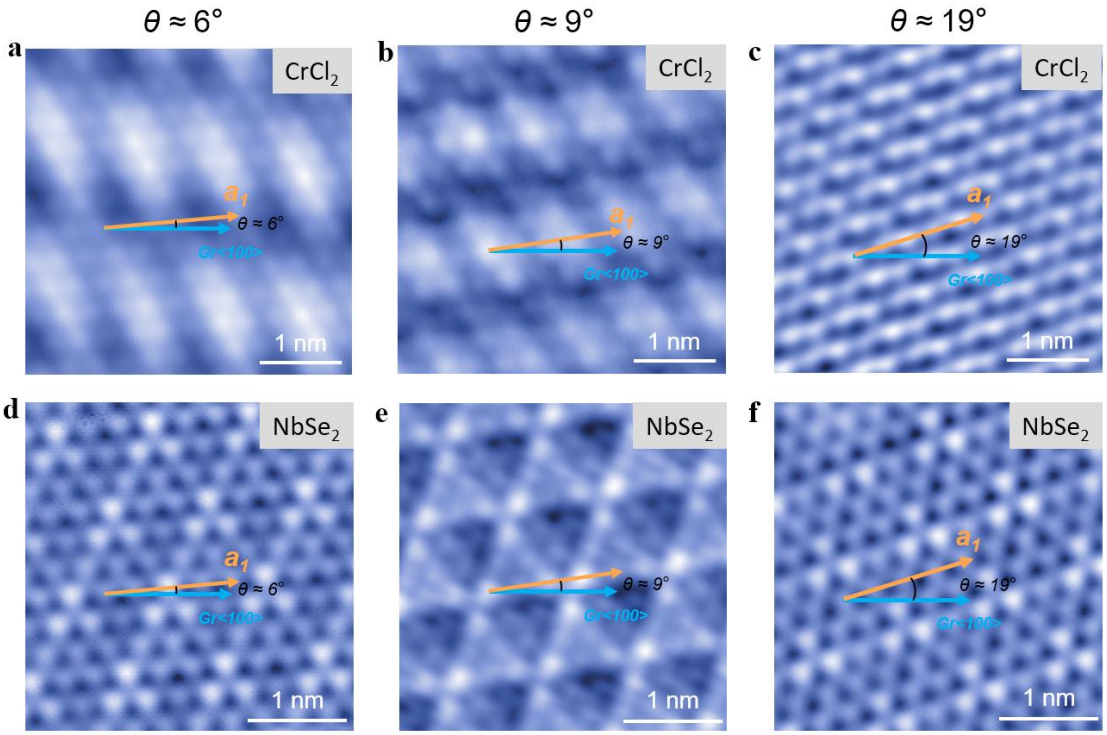

Figure S5 | Monolayer $CrCl_2$ aligns in the same direction as $NbSe_2$. a-c, STM topography images showing the moiré superlattices of $CrCl_2$ with twist angles (V_{Bias} = 0.4V, I_t = 10 pA). **d-f,** STM topography images showing the $NbSe_2$ with twist angles. Monolayer $CrCl_2$ aligns in the same direction as $NbSe_2$ (V_{Bias} = 0.1V, I_t = 50 pA). It indicates that the direction of $CrCl_2$ is determined by $NbSe_2$. In addition, $NbSe_2$ grown on graphene will have various rotation angles, which is consistent with the reference 33.

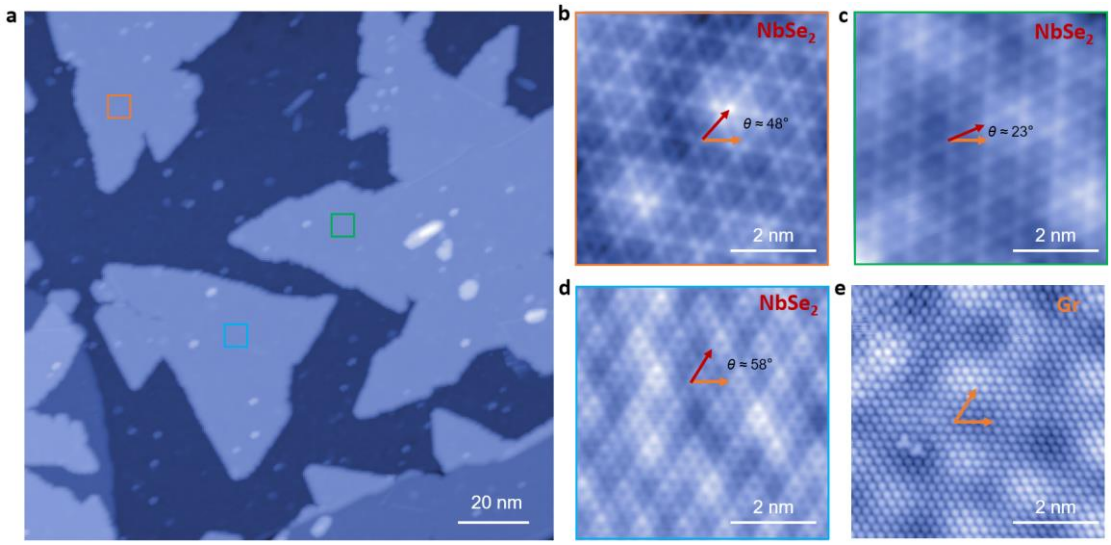

Figure S6 | Rotational orientation of monolayer $NbSe_2$ on graphene. a, STM morphology of $NbSe_2$ grown on graphene (V_{bias} = 1.5 V, I_t = 5 pA). **b-d**, Atomically resolved images of the monolayer $NbSe_2$ (V_{Bias} = 0.1V, I_t = 50 pA). **e**, Atomically resolved images of the graphene (V_{Bias} = 0.1V, I_t = 50 pA).

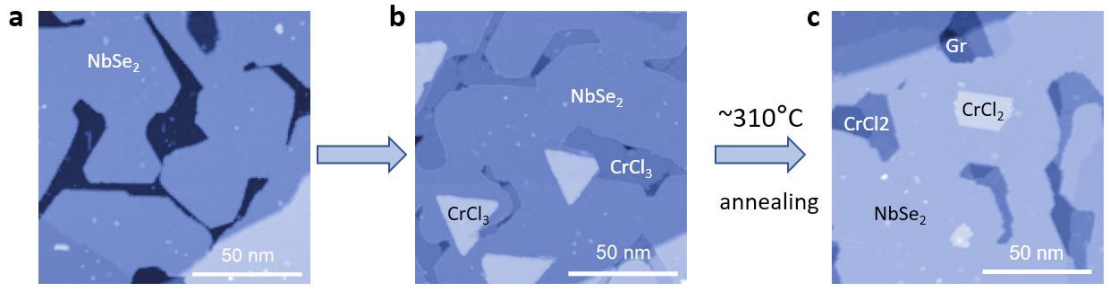

Figure S7 | Monolayer $CrCl_2$ grown on monolayer $NbSe_2$. a, STM morphology of $NbSe_2$ grown on graphene. **b**, STM morphology after the growth of $CrCl_3$. **c**, STM morphology after annealing. Scanning parameters for all images: V_{bias} = 1.5 V, I_t = 5 pA. To identify the source of the conduction peak, we conducted a control experiment using $NbSe_2$ as the substrate, where $CrCl_2$ and $NbSe_2$ form a vertical heterojunction. To obtain $CrCl_2$ on the ML $NbSe_2$ substrate, we first grew $NbSe_2$ to a coverage of nearly one layer, followed by the deposition of $CrCl_3$. After annealing, we successfully created a $CrCl_2/NbSe_2$ vertical heterojunction on this control sample. The spectrum of $CrCl_2$ on $NbSe_2$ was subsequently measured from this sample.

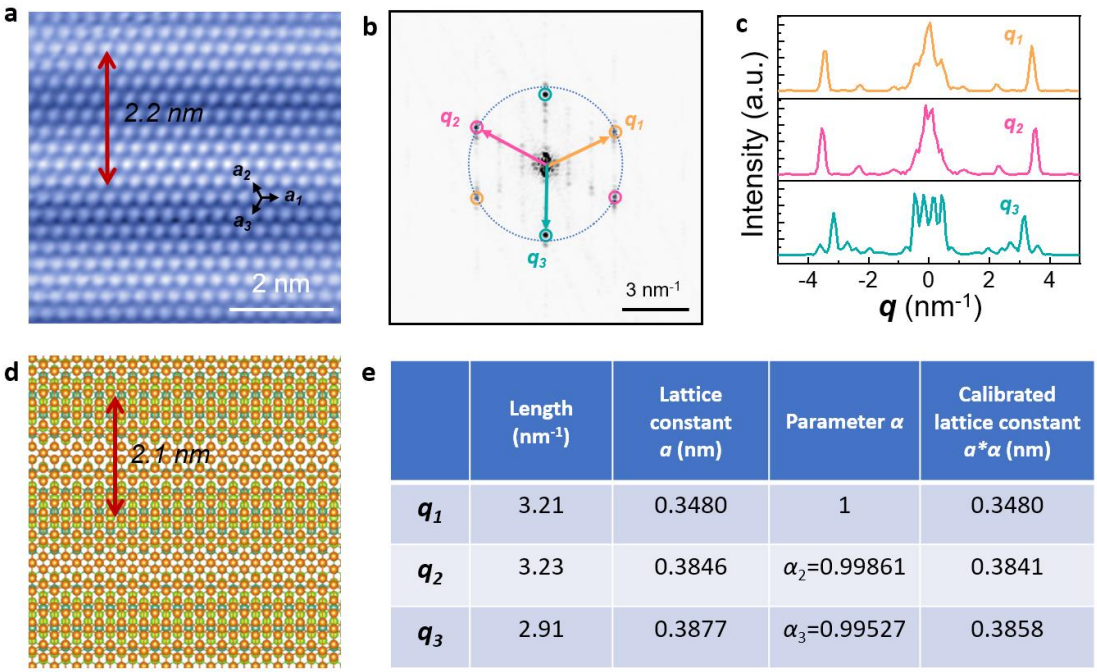

	Length (nm^{-1})	Lattice constant a (nm)	Parameter α	Calibrated lattice constant $a*\alpha$ (nm)
q_1	3.21	0.3480	1	0.3480
q_2	3.23	0.3846	α_2=0.99861	0.3841
q_3	2.91	0.3877	α_3=0.99527	0.3858

Figure S8 | Lattice constant of $CrCl_2$ on monolayer $NbSe_2$. a, Atomic resolution image of $CrCl_2$ lattice on monolayer $NbSe_2$ with stripy patterns, setpoint: V_{Bias} = 0.1 V, I_t = 50 pA. **b**, FFT of (a). **c**, Line profiles along the q_1, q_2 and q_3 directions marked in (b). **d**, The schematic models of $CrCl_2$ lattice on monolayer $NbSe_2$ showing the stripy patterns are moiré patterns. **e**, Calibration of the lattice constant.

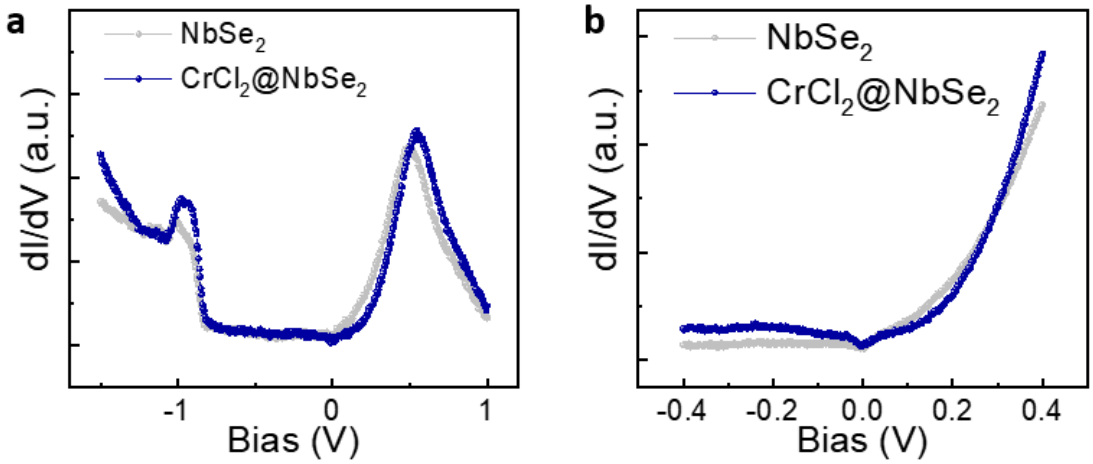

Figure S9 | dI/dV curves of $CrCl_2$ on $NbSe_2$ and nearby $NbSe_2$. a, The dI/dV curves taken on the $CrCl_2$ and nearby $NbSe_2$ regions, respectively. The measured dI/dV curve in the $CrCl_2$ band gap is almost consistent with the dI/dV curve of the nearby $NbSe_2$, which further proves that we can measure the density of states of the $NbSe_2$ underneath. **b**, The dI/dV curve within a small bias range around the Fermi level. Different from the measurement of $CrCl_2$ on graphene, a series of peaks are not observed.